CCUS: 4012771

Repeatability indicators in time lapse seismology and their application to the Sleipner CO_2 storage project

Brian Russell*
GeoSoftware, Calgary, Alberta, brian.russell@geosoftware.com

Abstract

I compare three repeatability measures using the time lapse data from Sleipner CO_2 storage project in offshore Norway. The three repeatability are *NRMS*, predictability, and cross-correlation coefficient. I first review the work of Kragh and Christie (2002) who used *NRMS* and predictability and created a random noise model to explain their relationship. Using the Sleipner dataset, I show an excellent fit to their theory. I then review the work of Coléou et al. (2013), who used *NRMS* and cross-correlation measures and introduced two new attributes: quality indicator (Q) and anomaly indicator (A). After discussing the relationship between predictability and cross-correlation I apply the Q and A attributes to the Sleipner dataset, showing how well the CO_2 plume can be identified.

Introduction

As shown in Figure 1 (Ghaderi and Landrø, 2009), the Sleipner storage CO_2 project is roughly halfway between Scotland and Norway, in the Norwegian sector of the North Sea. In this project CO_2 is separated from the produced gas in the Sleipner West Gas Field and injected into the Utsira saline formation. The Utsira formation is 800-1000 m deep, highly porous (36-40%) and permeable (1-8 D). Approximately 1 million tons of CO_2 per year has been injected into Sleipner since 1996. By 2010, 12 Mt of CO_2 had been injected into the reservoir.

Seismic monitoring started with a base survey in 1984, before injection. Monitor surveys were done in 1999, 2001, 2004, 2006, 2008, and 2010. This 4D dataset was released to the public by Equinor and is freely downloadable. The Sleipner seismic dataset consists of 28 volumes, the full,

near, mid, and far stacks for each of the seven vintages of data: 1994,1999, 2001, 2004, 2006, 2008 and 2010.

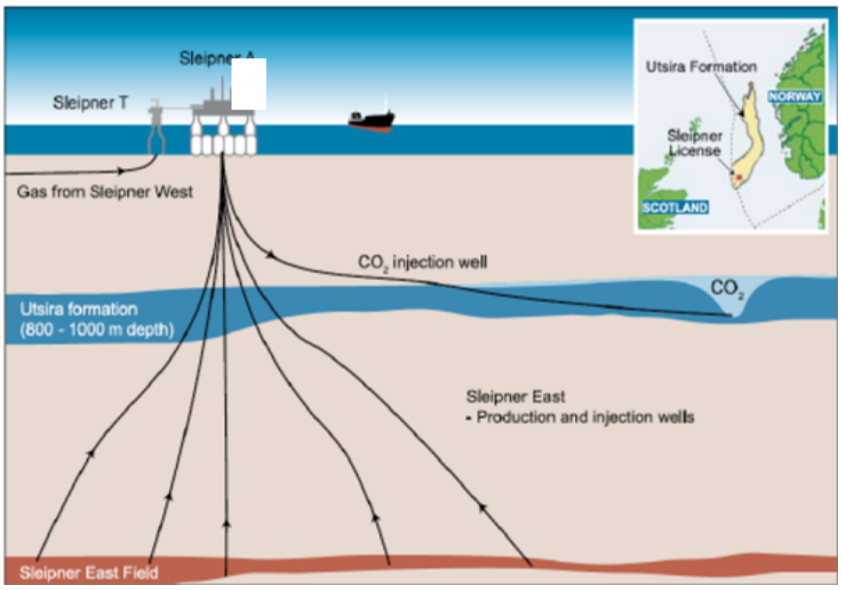

Figure 1. Geology of the Sleipner CO_2 storage project (Ghaderi and Landrø, 2009).

In this study, I will apply several repeatability measures to the base and monitor surveys to analyze the footprint of the injected CO_2.

Theory

The three repeatability measures I will use in this study are the normalized root-mean-square (*NRMS*) approach, predictability (*PRED*), and cross-correlation coefficient (ρ). Let's first review the work of Kragh and Christie (2002) who used *NRMS* and *PRED* as their two indicators. *NRMS* between the base (b) and monitor (m) surveys is defined as

$$NRMS = \frac{200\left[RMS(m-b)\right]}{RMS(m)+RMS(b)}, \tag{1}$$

where $RMS(x_t) = \sqrt{\frac{1}{N+1}\sum_{t=t_0}^{t_N} x_t^2}$ is the RMS estimate over trace samples x_t using a time window from time $t = t_0$ to $t = t_N$. Note that the limits of the *NRMS* are from 0 to 200.

The predictability, or *PRED*, is defined as

$$PRED = \frac{\sum_{\tau=-\max lag}^{\max lag} \phi_{bm}{}^2(\tau)}{\sum_{\tau=-\max lag}^{\max lag} \phi_{bb}(\tau) \sum_{\tau=-\max lag}^{\max lag} \phi_{mm}(\tau)}, \tag{2}$$

where $\phi_{bm}(\tau)$ is the cross-correlation between the base and monitor traces from lags between -and +max lag, $\phi_{bb}(\tau)$ is the autocorrelation of the base trace, and $\phi_{mm}(\tau)$ is the autocorrelation of the monitor trace between the same lags. The limits of the predictability are from 0 to 100%.

Kragh and Christie (2002) then show that the relationship between *NRMS* and *PRED* can be computed theoretically when adding random, or white, noise to a reference trace, and comparing the noisy trace to the original reference trace. The formulae for the two repeatability measures are given as

$$NRMS = \frac{141}{\sqrt{1+\frac{1}{\lambda^2}}}, \text{ and} \tag{3}$$

$$PRED = \frac{100}{\left(1+\lambda^2\right)^2}, \tag{4}$$

where λ is the ratio of the white noise amplitude to the seismic amplitude. Notice that the highest value of *NRMS* is now 141 rather than 200, which comes from the theoretical definition of signal-to-noise ratio. To visualize these relationships, Figure 2 shows a plot of *PRED* versus *NRMS* for values of λ from 0.01 to 10. Notice that this plot is Gaussian, or bell-shaped. In the next section I will show that the real data cross-plots derived from the Sleipner dataset conform extremely well to this theoretical shape.

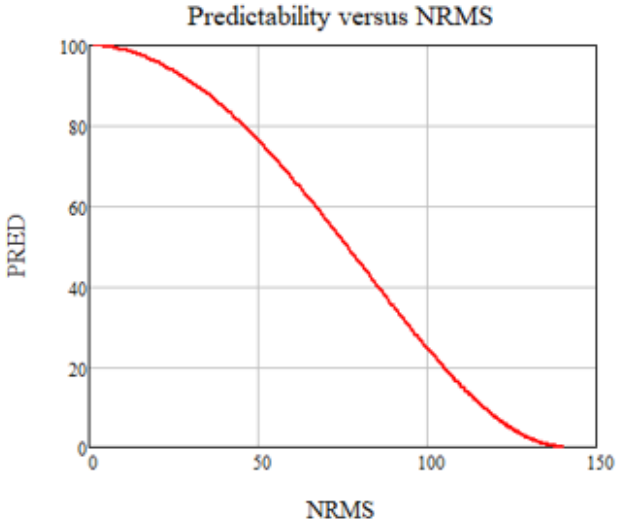

Figure 2. Plots of PRED versus NRMS from the relationships in equation 3 and 4.

The third repeatability indicator, correlation coefficient, or ρ, is the ratio of the maximum cross-correlation value at lag t_{max} divided by the product of the square roots of the autocorrelations, or

$$\rho = \frac{\phi_{bm}(\tau_{\max})}{\sqrt{\phi_{bb}(\tau_{\max})}\sqrt{\phi_{mm}(\tau_{\max})}}. \tag{5}$$

Equation 5 finds a single correlation coefficient, whereas the predictability in equation 2 computes an *RMS* average over a series of lags. The advantage of using cross-correlation is that the time shift t_{max} between the base and monitor surveys can be used to align the two surveys. The advantage of the predictability measurement is that it gives a smoothed correlation result.

To quantify the amount of smoothing that occurs when using predictability as compared to correlation coefficient with, Kragh and Christie (2002) assume that the effect the number of lags used in the computation of predictability can be simulated by adding a damping factor to equation 4, or

$$PRED = \frac{100}{\left(1 + d\lambda^2\right)^2}, \tag{6}$$

where d is the damping factor.

Coléou et al. (2013) extended the work of Kragh and Christie (2002) by considering the statistics behind ρ and *NRMS* and using these two measures in their cross-plot. Figure 3 shows a set of points from a 4D survey with two solid curves and a set of dashed lines superimposed. Figure 3(a) is a plot of correlation coefficient versus $NRMS^2/2$ and Figure 3(b) is a plot correlation coefficient versus *NRMS*. Notice that the Kragh and Christie (2002) limits have been normalized by dividing by 100.

The dashed curves in Figure 3 represent what Coleou et al. (2013) call quality indicator, or Q, which will be defined shortly. The solid red curve is the lower bound when the two datasets have the same variance, and can be written as

$$\rho = 1 - \frac{NRMS^2}{2}. \tag{7}$$

Euqation 7 shows why Figure 3(a) had $NRMS^2/2$ on the x axis, since the curve us linear with respect to $NRMS^2/2$. The solid green curve is the lower bound when we add random noise to a seismic trace and compare the traces, and can be written as

$$\rho = \frac{4 - NRMS^2}{4 + NRMS^2}. \tag{8}$$

The green curve in Figure 3(b) is almost identical to Kragh and Christie's equation with a damping factor of 0.5, as given in equation 6.

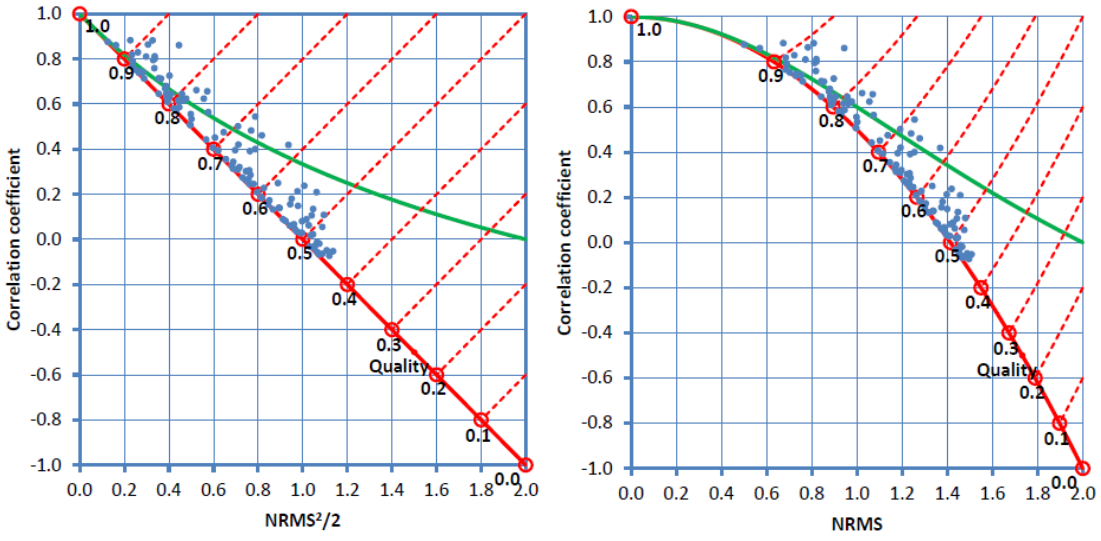

(a) (b)

Figure 3. Plot of (a) ρ vs NRMS^2/2, and (b) ρ vs NRMS, showing lines of constant Q (Coléou et al., 2013).

Coléou et al. (2013) also introduced two new repeatability indicators. The first is called the quality indicator, Q, which is shown by the dashed red lines in Figure 3, and which is defined mathematically as

$$Q = \frac{\rho - NRMS^2/2}{4} + \frac{3}{4}, \tag{9}$$

where $NRMS = \frac{2\sigma(b-m)}{\sigma(b)+\sigma(m)}$, $\rho = \frac{Cov[b,m]}{\sigma(b)\sigma(m)}$, σ = standard deviation, and Cov = covariance, and b and m are the base and monitor surveys. I have arranged equation 9 slightly differently than Coléou et al. (2013) to make it more interpretable. Notice that the equation consists of the difference between ρ and $NRMS^2/2$ divided by 4 with an added term of 3/4. Equation 9 explains the dashed red lines on Figure 3(a), which represent lines of constant Q. Consider the line extending at right angles from $Q = 0.5$. When $NRMS^2/2 = 1$ and $\rho = 0$, we see that $Q = -1/4 + 3/4 = 1/2$. But when $NRMS^2/2 = 2$ and $\rho = 1$, we see that $Q = -1/4 + 3/4 = 1/2$ as well.

The second indicator defined by Coléou et al. (2013) is called the anomaly indicator A, which is defined mathematically as

$$A = \frac{\rho + NMRS^2/2}{2} - \frac{1}{2}, \tag{10}$$

Again, I have arranged equation 10 slightly differently than Coléou et al. (2013) did to make it more interpretable. This equation differs from equation 9 in that it consists of the sum of ρ and $NRMS^2/2$, rather than the difference, which is divided by 2 and has a subtracted term of 1/2. Figure 4(a) shows a plot of ρ versus $NRMS^2/2$ and Figure 4(b) shows a plot of ρ versus $NRMS$, where both plots now show lines of constant A.

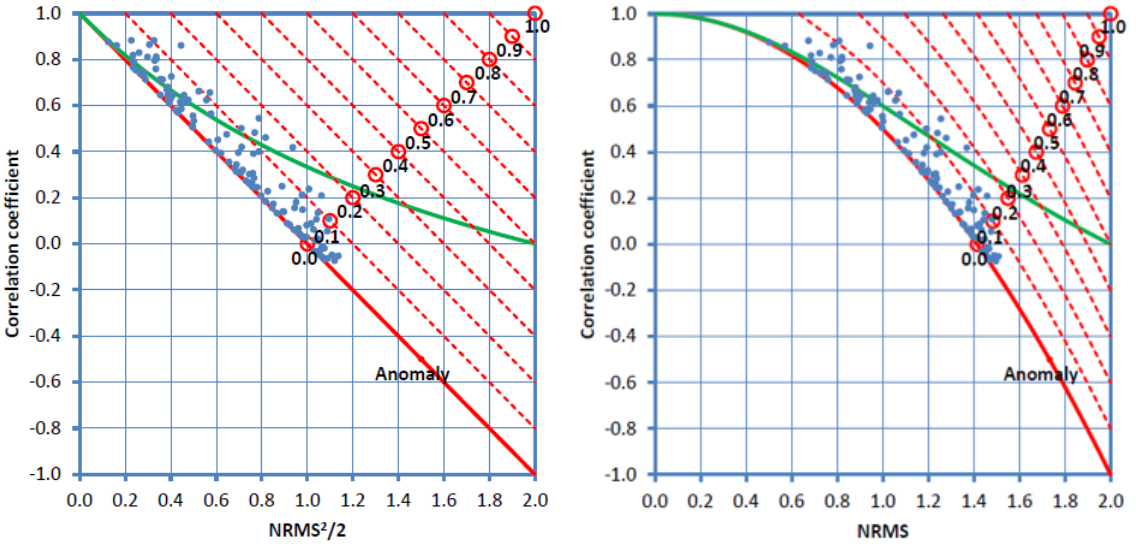

Figure 4. Plot of (a) ρ vs NRMS^2/2, and (b) ρ vs NRMS, showing lines of constant A (Coléou et al., 2013).

The best way to understand that the anomaly indicator A is defined by parallel lines rather than orthogonal lines, as in the quality indicator Q, is to substitute values into equation 11. For example, if we look at the solid line where $A = 0$, note that for $NRMS^2/2 = 1$ and $\rho = 0$, we get $A = 1/2 - 1/2 = 0$, and that when $NRMS^2/2 = 2$ and $\rho = 1$, we again get $A = 1/2 - 1/2 = 0$. But as we move to larger values of $NRMS^2/2$, this constant value is shifted from zero to larger values. Thus, the A indicator is orthogonal to the Q indicator. In the next section, we will apply the theory of both Kragh and Christie (2002) and Coléou et al. (2013) to the Sleipner dataset.

Results

First, let's look at the method proposed by Kragh and Christie (2002). Figure 5 shows the *NRMS* differences between the base and monitor surveys for the CO_2 injection project at Sleipner. These differences were computed over 1200 msec window between times of 400 and 1600 msec. Note the excellent definition of the expanding CO_2 plume using this repeatability indicator.

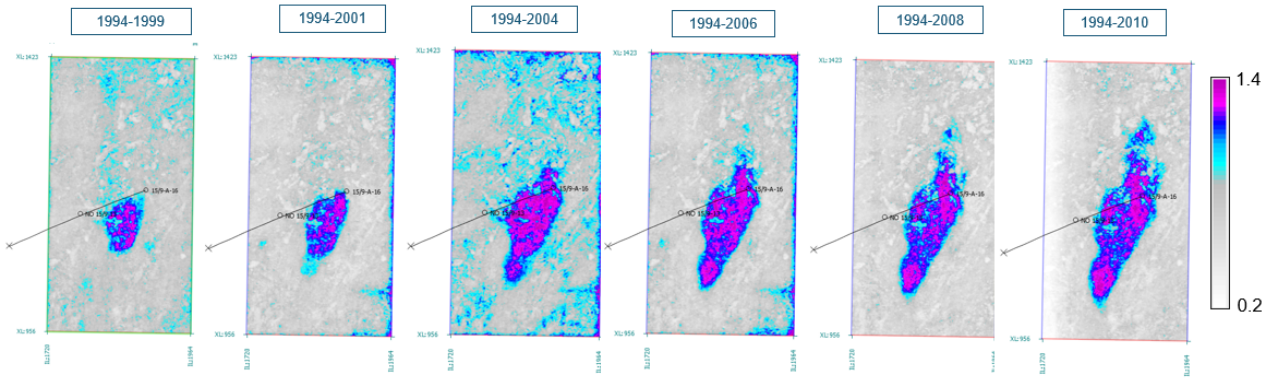

Figure 5. Plot of the *NRMS* difference between the base and monitor surveys for the CO_2 injection project at Sleipner.

Figure 6 shows the predictability differences between the base and monitor surveys for the CO_2 injection project at Sleipner, again computed over a 1200 msec window between times of 400 and 1600 msec. Again, note the excellent definition of the expanding CO_2 plume using this repeatability indicator. The colour scale in Figure 6 is the reverse of the colour scale shown in Figure 5 to show that the anomalous zones have high values of NRMS but small values of predictability.

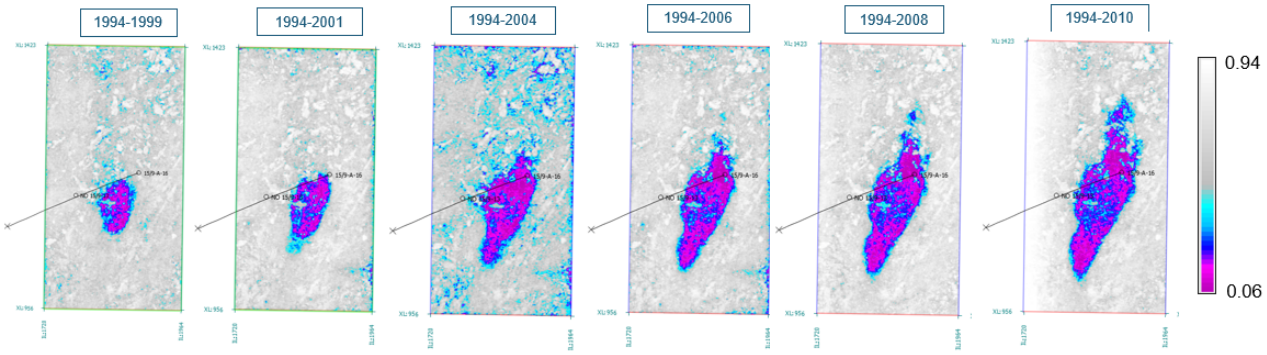

Figure 6. Plot of the predictability differences between the base and monitor surveys for the CO_2 injection project at Sleipner.

Figure 7 shows a cross-plot of *PRED* vs *NRMS* for the 1994 to 2010 survey comparison, where the colour represents crossline number. Notice the excellent agreement between the theory from the previous section (since we expect a Gaussian-type shape) on the data display. On this plot, I have picked an elliptical zone on the cross-plot using the anomalous points with low predictability and high *NRMS*, using the central crosslines. Notice how well the CO_2 plume is defined by this zone.

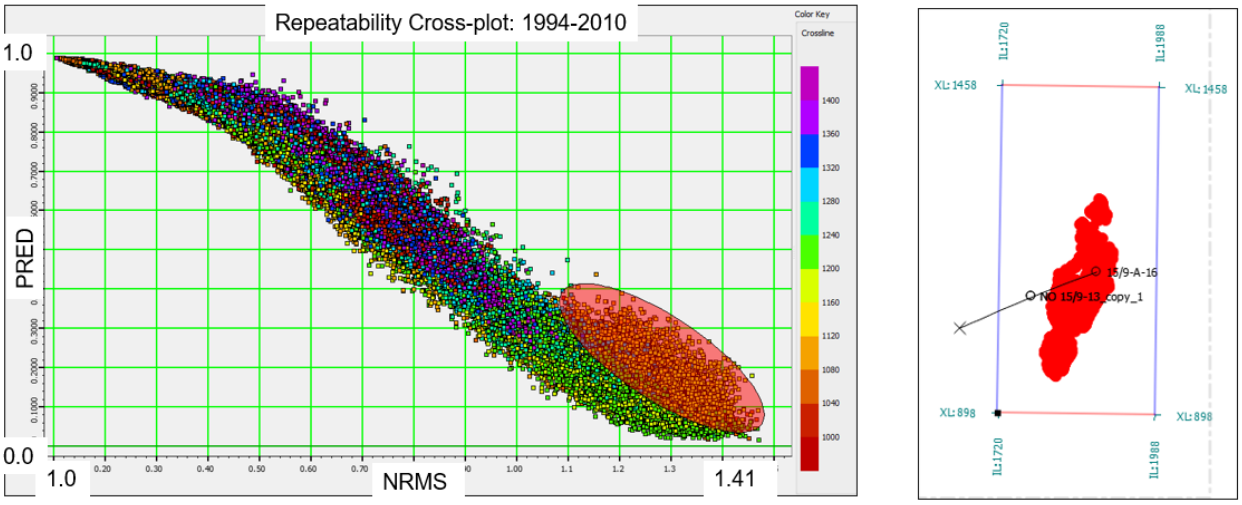

(a) (b)

Figure 7. (a) A cross-plot of predictability against *NRMS*, with an elliptical zone picked around the central crosslines, where (b) shows the anomalous zone.

Next, let's apply the indicators defined by Coléou et al. (2013). The correlation coefficient between the base and monitor surveys for Sleipner is shown in Figure 8, where the value ranges from 0 (no correlation) to 1 (perfect correlation). These differences were computed over 1200 msec window between times of 400 and 1600 msec, as was done for both the *NRMS* and predictability results shown earlier. The expanding injection plume is clearly defined by low cross-correlation values.

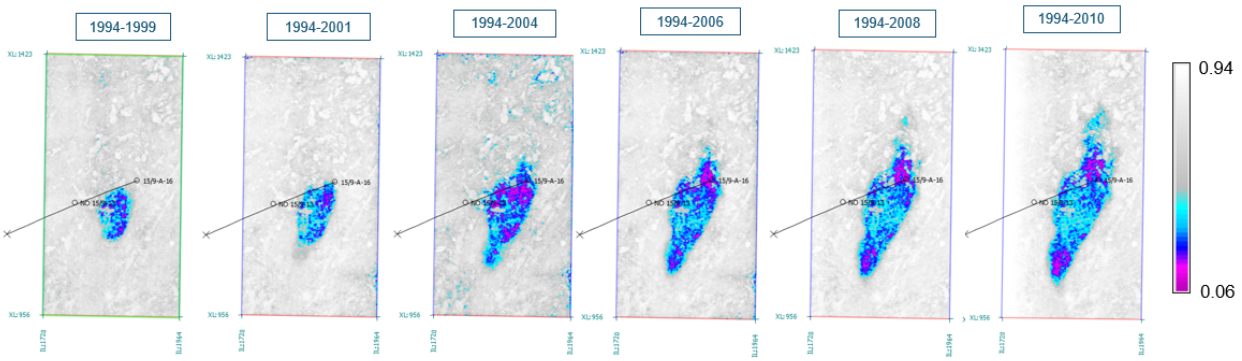

Figure 8. The correlation coefficient between the base and monitor surveys for Sleipner.

Figure 9(a) shows a cross-plot of ρ versus *NRMS* between 1994 and 2010, with the colour scale representing crosslines. Note how well the lower limit of the plot corresponds to the theory. Figure 9(a) also shows an elliptical zone picked on the cross-plot using the middle crosslines. Figure 9(b) shows the points from the anomalous region projected onto the seismic map, which corresponds very closely to the injection plume.

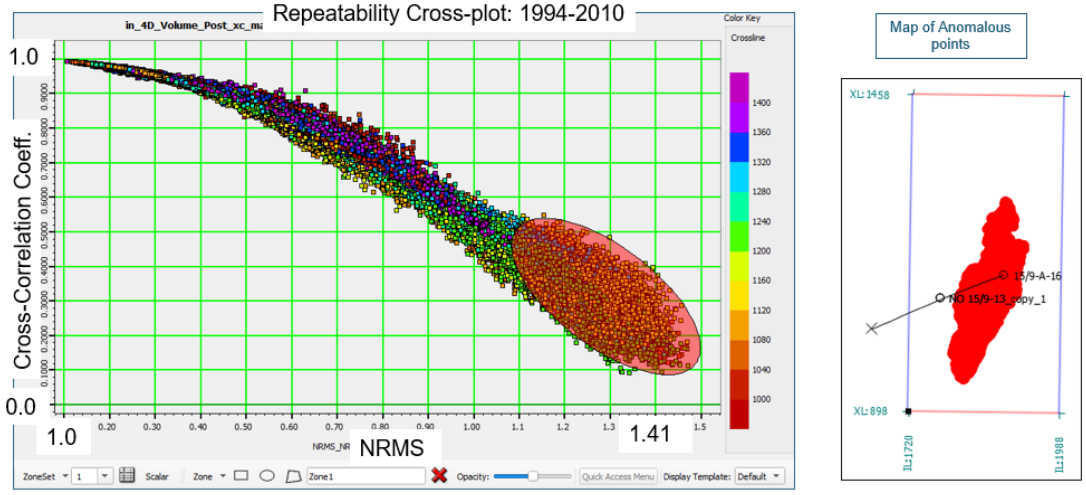

(a) (b)

Figure 9. (a) An elliptical zone around the central crosslines with an elliptical zone picked where (b) shows the anomalous points.

Next, I created the quality indicator (Q) map and the anomaly indicator (A) map, using the mathematical relationships given in equations 9 and 10. These two maps are shown in Figures 10(a) and (b).

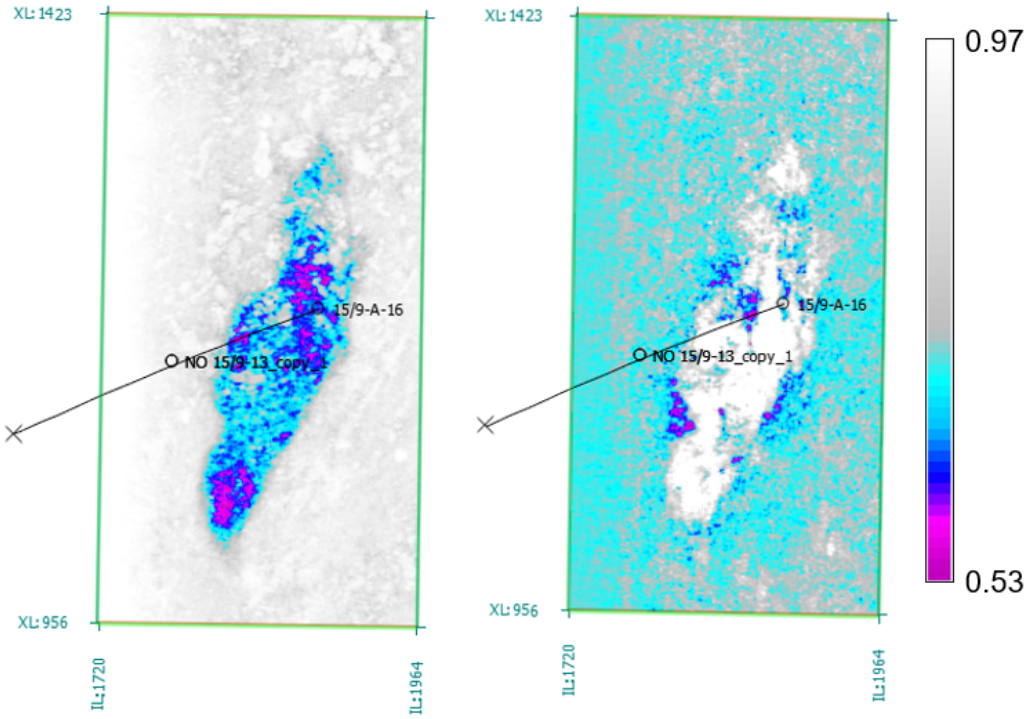

(a) (b)

Figure 10. (a) Quality indicator (Q) map, and (b) anomaly indicator (A) map.

The quality indicator map is similar to the cross-correlation map, but the anomaly indicator shows some interesting features not seen in previous maps.

Next, I cross-plotted the two maps from Figure 10. Figure 11 shows the cross-plot of the two new attributes with *Q* shown on the vertical axis and *A* shown on the horizontal axis. The histograms of the two attributes are also shown. In Figure 11(a), the low values of *Q* from the cross-plot have been picked with an elliptical zone, which correspond to the CO_2 plume, as shown in Figure 11(b)

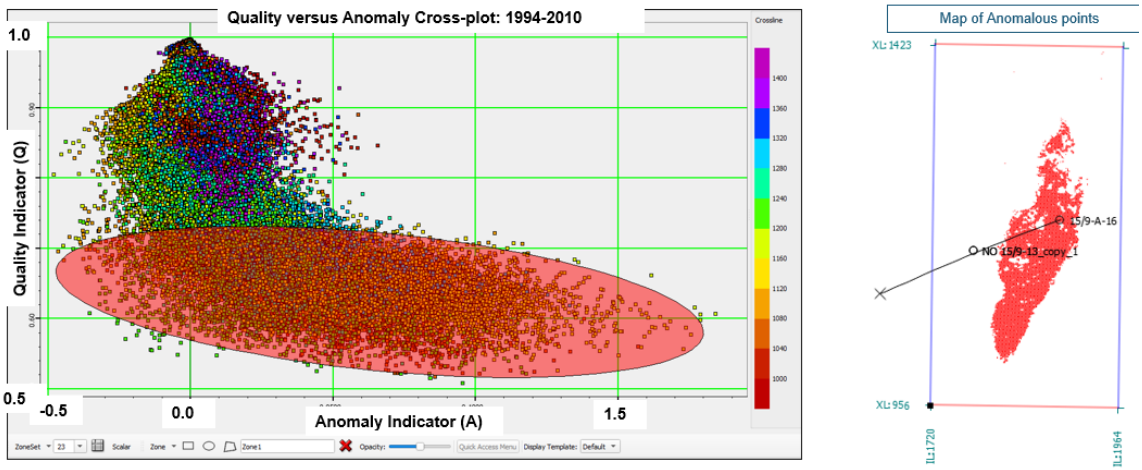

(a) (b)

Figure 11. (a) An elliptical zone around the central crosslines in the plot of Figure 21, where (b) shows the anomalous zone.

Finally, Figure 12(a) shows four picked rectangular zones from the cross-plot of Figure 11, where Figure 12(b) shows the corresponding mapped areas.

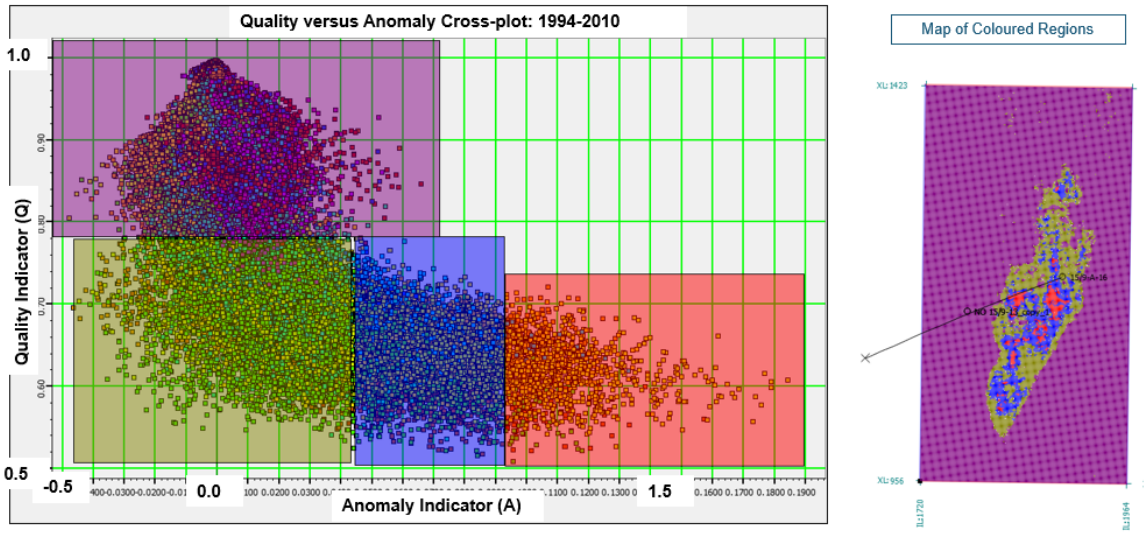

(a) (b)

Figure 12. (a) Four rectangular zones have been picked on the plot of Figure 22, where (b) shows the anomalous zone.

In the map of Figure 12(b), we can now clearly see multiple zones within the anomalous area, where the purple zone defines the non-anomalous area and the green, blue, and red zones define areas of interest within the anomalous area.

Discussion

In this study I have computed and compared five different repeatability measures using the time lapse data from Sleipner CO_2 storage project in offshore Norway. These repeatability measures were *NRMS*, predictability, and cross-correlation coefficient, or ρ, quality indicator (Q) and anomaly indicator (A) which, as shown by Coléou et al. (2013), were weighted combinations of *NRMS* and ρ.

Note the similarity of the cross-correlation coefficient and quality indicator maps, and between the *NRMS* and predictability maps (although the colour scales are reversed in these two maps, since on *NRMS* the high values are anomalous and on predictability the low values are anomalous). However, the anomaly indicator map shows interesting features, suggesting it may be a useful new indicator to use. The real power of these plots is when they are cross-plotted and interrogated using interactive zone picking, as shown in Figures 11 and 12. The zones in Figure 12(b) could be matched up with different amount of injected CO_2 within the storage area, and future research will try to identify such zones.

Conclusions

In this study, I compared repeatability measures using the time lapse data from Sleipner CO_2 storage project in offshore Norway. I first reviewed the work of Kragh and Christie (2002) who cross-plotted *NRMS* and predictability and created a random noise model to explain the relationship between the two indicators. Using the Sleipner dataset, I was able show an excellent fit to their theory.

I next reviewed the work of Coléou et al. (2013), who used a cross-plot of *NRMS* versus cross-correlation coefficient. Coléou et al. (2013) also introduced two new attributes: Quality Indicator (Q) and anomaly indicator (A). After discussing the relationship between predictability and cross-correlation I then analyzed the mathematics behind the Q and A indicators and applied these indicators to the Sleipner dataset. For each repeatability indicator the anomalous CO_2 plume in Sleipner as a function of time lapse study could be identified, and each indicator gave us a unique perspective on the morphology of the CO_2 injection zone.

References

Ghaderi, A., and Landrø, M., 2009, Estimation of thickness and velocity changes of injected carbon dioxide layers from prestack time-lapse seismic data: Geophysics, **74**, O17-O28.

Kragh, E., and Christie, P., 2002, Seismic repeatability, normalized rms, and predictability: The Leading Edge, **21**, 640 – 647.

Coléou, T., Coulon, J-P, Carotti, D., Dépré, P., Robinson, G, and Hudgens, E, 2013, AVO QC during processing: Presented at the 75th EAGE Conference, London, UK.